Hindawi
Mathematical Problems in Engineering
Volume 2020, Article ID 1975428, 9 pages
https://doi.org/10.1155/2020/1975428

Research Article

Elastostatic Stiffness Analysis for the US/UPS Parallel Manipulators

Weizhong Zhang,[1,2] Wei Ye,[1] and Chao Yang[3]

[1]*Faculty of Mechanical Engineering and Automation, Zhejiang Sci-Tech University, Hangzhou 310058, Zhejiang, China*
[2]*Faculty of Automation, Zhejiang Institute of Mechanical and Electrical Engineering, Hangzhou 310018, Zhejiang, China*
[3]*College of Mechanical and Electrical Engineering, Jiaxing University, Jiaxing 314003, Zhejiang, China*

Correspondence should be addressed to Chao Yang; cyang@zjxu.edu.cn

Received 21 April 2020; Revised 8 June 2020; Accepted 11 June 2020; Published 13 July 2020

Guest Editor: Carlos Llopis-Albert

The virtual joint method (VJM) cannot calculate the strain energy stored in each rod. In order to solve the problem, a modeling method of the elastostatic stiffness was investigated for the UP/UPS parallel manipulators (PMs), taking the example of the 6-SPS PM. The modeling method was based on screw theory, Castigliano's theorem, and strain energy (where U, P, and S, respectively, denote universal, prismatic, and spherical joints). First, the actuator and constraint wrenches of the mechanism were obtained by screw theory. Second, compact limb stiffness matrices were obtained in terms of strain energy and Castigliano's second theorem. Finally, analytic expressions for the overall stiffness matrix of the mechanism and the amplitudes of the actuator force were obtained by adopting the virtual work principle and the balance equation for the mobile platform. All relative errors between the results of the analytical model and the finite element model are below 2%, which validates the effectiveness of the elastostatic stiffness model. The virtual work index was adopted to evaluate the stiffness performance of the mechanism, and the results show that the stiffness is not only related to position and orientation but also closely related to the directions of external loads. It is also demonstrated that the method has general adaptability for the stiffness analysis for the US/UPS PMs, laying the foundation for further reasonable dynamic design and optimization of such manipulators.

1. Introduction

Compared with serial manipulators, PMs with closed kinematic structures perform well in terms of accuracy, rigidity, and payload capacity and show high potentials to deal with numerous tasks [1–3]. Therefore, the detailed analyses of PMs are extremely important, including the workspace [4], kinematics [5], dynamics [6], elastostatics [7], and motion/force transmissibility [8].

As an essential class of the UP/UPS PMs, the 6-SPS PM is an example of successful engineering applications [9], including parallel robotic manipulators [10], positioning devices [11], remote center-of-compliance devices [12], minimally invasive surgeries [13], and haptic interface mechanisms [14]. The 6 degrees of freedom (DOFs) of the Stewart PM based on the 6-SPS PM [15] are well known as a typical example to provide enough orientation capability and high stiffness, and it has been widely used in many industrial applications, for example, the flight simulators [16].

To meet the demand for high precision from the industry, the stiffness analysis of PMs is also essential in the pre-design stage, which should consider the influences of joints and links, and is also the basis of the multi-objective optimization and structural design of PMs [17, 18]. Considering the influence and importance of stiffness on the precision of PMs, many progresses have been presented by the academic community for the stiffness characteristics of PMs, which are focused on the various methods of the stiffness modeling and performance evaluation index [19–23].

Although the stiffness of the 6-SPS PM can be numerically simulated by using the finite element analysis (FEA)

software, from which the results with high accuracy can be obtained, the process using the FEA software is very time-consuming, and it has to rebuild the model under different configurations [24, 25]. Therefore, developing the analytical or semi-analytical models in the pre-design stage is a better choice for estimating the stiffness characteristics of the Stewart PMs in the whole workspace [26]. Some analytical studies about the stiffness analysis of the Stewart PM have been proposed. Using the kinematics error model of the Stewart robot, Ding et al. analyzed the stiffness performance of the Stewart PM equipped with decoupled sensors and actuators [27]. Additionally, the FEA method under the action of (nanoscale) ultrahigh accuracy positioning and the large external load was used to verify the stiffness results. Adam et al. analyzed and evaluated the stiffness matrix of a double Stewart PM truss adopting an analytical method [28]. Based on the principle of linear superposition, Li et al. studied and established the stiffness matrix of the Stewart platform by considering the deformation of the mechanism support [29]. Svinin et al. analyzed the stiffness and stability of the Stewart PM under the condition of internal forces preloading [30]. Huang et al. considered the flexibility factor of the Stewart PM using the law of the conservation of energy and proposed a new conservative stiffness mapping [31]. They captured the compliance characteristics of the mechanism using an additional stiffness matrix. Moreover, since the rod of two-force only subjected to tension and compression, the virtual joint method is used to analyze the elastostatic stiffness performance of PMs [32, 33].

Besides the stiffness modeling, the evaluation of stiffness performance is also essential for ensuring that the performance meets the requirement [34, 35]. The stiffness matrix of the PMs is a 6×6 mapping matrix, which can evaluate the relationships between the external wrenched and infinitesimal deformations. To evaluate the stiffness performance of the PMs, the stiffness matrix must be transformed into a quantifiable index [36, 37]. The most used stiffness indices at present include the determinant of the stiffness matrix [38], the average value of the eigenvalues [39], the maximum and minimum eigenvalues [40], and the ratio of the minimum and maximum eigenvalues [41]. However, owing to the different units used for position and orientation, there is a common shortcoming of all the above indices; i.e., the dimensions are not uniform, and the index values cannot be well illustrated. The virtual work index (VWI), used in this paper, is reciprocal of the virtual work done by the external load [35]. In contrast to the case for other indices, the units of position and orientation are uniformly used as virtual work within the VWI. Additionally, the VWI can be used to measure the deformation of PMs resisting external load in a specific direction.

In order to solve the problem of the fact that the virtual joint method cannot calculate the strain energy stored in each rod, the main content of this paper is to investigate a modeling method for elastostatic stiffness analysis for the UP/UPS PMs, taking the example of the 6-SPS PM, which is based on the screw theory, Castigliano's theorem, and strain energy method. Through calculating the strain energy stored in each rod, the stiffness matrices of each rod and PMs can be obtained, which have a clear physical meaning and concise expression.

The remainder of the paper is organized as follows. Section 2 adopts screw theory, strain energy, and Castigliano's second theorem to derive a general analytical expression for the stiffness matrix of the limb of the 6-SPS PM. The elastostatic stiffness of the 6-SPS PM using the proposed method was analyzed. Section 3 uses the finite element commercial software ANSYS to develop FEA models in different configurations with external wrenches and makes a verification to show the correctness of the theoretical method. Based on the virtual work, Section 4 introduces and evaluates the stiffness performance of the 6-SPS PM by using VWI. Section 5 discusses the results of the simulation. Section 6 presents the conclusions of the study and suggestions for future work.

2. Elastostatic Stiffness Modeling for the 6-SPS PM

2.1. Process of Elastostatic Stiffness Modeling for the 6-SPS PM. Based on the strain energy method, Castigliano's second theorem, and the screw system of the limb stiffness matrix for the Stewart PM and the deformation coordination equation (DCE), the global stiffness matrix of parallel mechanism is derived [42]. The calculation process is shown in Figure 1.

At the same time, the constrained reaction force exerted on the mobile platform by the supporting limb is obtained. The calculation steps are described in detail as follows:

Step 1: using reciprocal screw theory, the constraint wrenches exerted on the mobile platform were defined by limbs $\$_{i1} = (\$_{i1}\$_{i2}\ldots)$

Step 2: based on the assumption of small deformations and the mechanics of the materials, we calculate the strain energy $U_i = f \times (f_{i2})$ of each supporting limb, where $f_i = (f_{i1} f_{i2})$ are the magnitudes of the limb constraint wrenches and U_i a function of f_i

Step 3: based on Castigliano's second theorem, the elastic deformation at the end of each limb in the direction of the screw axis of the constraint wrenches is calculated as follows: $(\delta_i = \delta_{i1}\delta_{i2}\ldots)$, where $\delta_{ij} = \partial U_i / \partial f_{ij}$

Step 4: we map elastic deformation δ_i to constraint wrenches f_i, namely, $\delta_i = C_i f_i$; the stiffness matrix of the limb can be obtained easily, namely, $\mathbf{K}_i = C_i^{-1}$

Step 5: the equilibrium equation of the mobile platform in a specific coordinate system was formulated, where $\mathbf{W} = G_f^F f$

Step 6: using the results from steps 4 and 5 along with the virtual work principle, the DCEs are obtained as $\delta_i = J_i^T \mathbf{D}$, $\mathbf{J}_i = (\$_{i1}^r \$_{i2}^r \ldots)$, where $\mathbf{D}$ is the infinitesimal twist of the geometric center point of the mobile platform and J_i is the mapping matrix between δ_i and $\mathbf{D}$

Step 7: using the DCEs, the overall stiffness matrix K is obtained, where $\mathbf{K} = \mathbf{J}_i \sum \mathbf{K}_i J_i^T$ $\mathbf{D} = \mathbf{K}^{-1}\mathbf{W}$

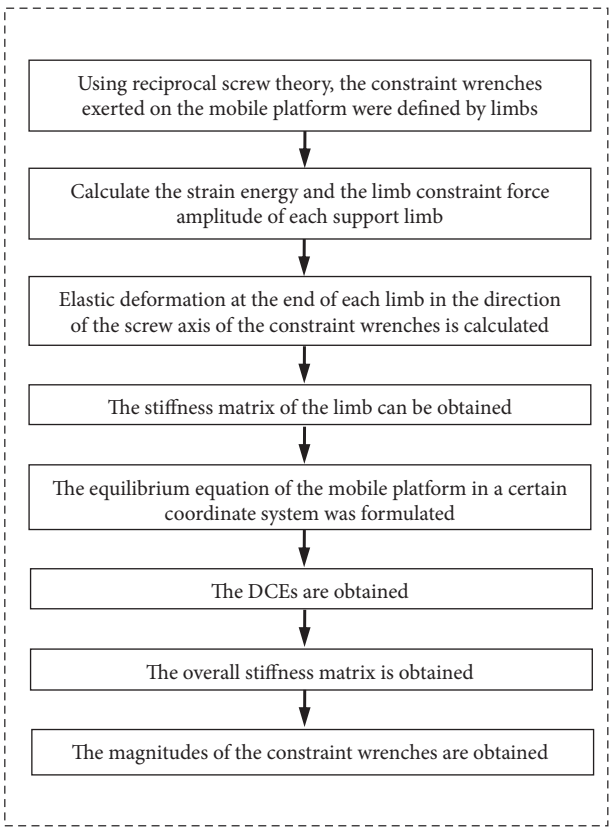

Figure 1: Calculation flow chart of the global stiffness matrix K.

Step 8: from matrix K, the magnitudes of the constraint wrenches are obtained, where $f_i = K_i\delta_i = \mathbf{K}_i J_i^T K^{-1}\mathbf{W}$

2.2. Description for the UP/UPS PMs. In the following, the application of the stiffness modeling method for the UP/UPS PMs is studied. The UP/UPS PMs feature a static platform and mobile platform connected through both links (legs) of type US having constant length and legs of type UPS having controllable distance, as shown in Figure 2.

A typical characteristic of the US/UPS PMS is the same topological structure within the workspace. In the process of parameterization, generalized matrices with the same independent variables and similar structures are analyzed. A class of three-degree-of-freedom (3-DOF) US/UPS PMs, in which the relative motion between the base and platform is spherical, has been proposed, where mechanisms belonging to this class have at least three legs of type US and only three legs of type UPS [43]. A class of 6-DOF US/UPS PMs, in which the relative motion between the base and platform is general, has been proposed, where mechanisms belonging to this class have legs of type UPS only [44].

The diagram of the model and the coordinate system of the 6-SPS PM are shown in Figure 3. Six identical linkages of the 6-SPS PM connect the mobile platform and static platform at B_i and A_i through a spherical joint. Both the mobile platform and static platform are semi-regular hexagons. The circumferential radius of the mobile platform and static platform is, respectively, denoted by R_b and R_a.

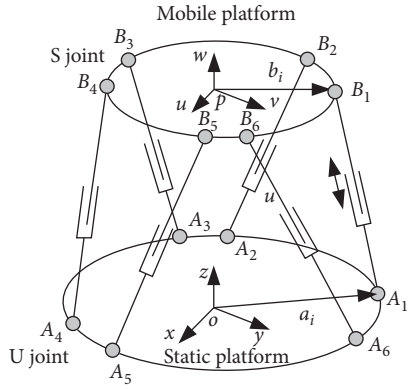

Figure 2: PM with legs of types US and UPS.

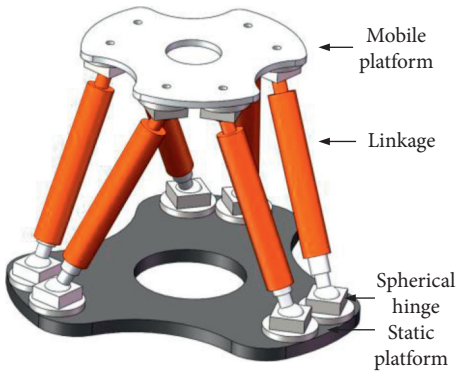

Figure 3: Diagram of the model for the 6-SPS PM.

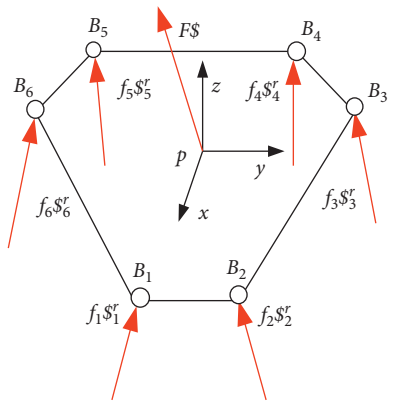

Figure 4: Force analysis chart of the mobile platform.

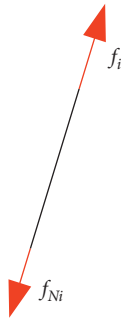

Figure 5: Free-body diagram and section view of the ith linear rod.

The center angles of the long sides A_1A_2 and B_2B_3 are β_0. As is well known, there are six SPS limbs for 6-SPS PM.

2.3. Stiffness Matrix of Each Limb for the 6-SPS PM. A force analysis diagram of the mobile platform of the 6-SPS PM is shown in Figure 4. The motion pairs of the limb from the base to the mobile platform are S pairs, P pairs, and S pairs. Each limb of the 6-SPS is subjected only to an axial force, resulting in the limb rod generating a tensile or compressive elastic deformation. According to the screw theory, there is a constrained wrench exerted on the SPS limb of the mobile platform along the center for the two S pairs. Therefore, the SPS rod can regard each limb as a two-force rod only subject to tension and compression. Force analyses of the SPS limb and mobile platform are shown in Figure 5:

$$f_{Ni} = f_i. \tag{1}$$

The strain energy of the SPS limb is given as

$$U_i = \frac{f_{Ni}^2 L_i}{2E_i A_i}, \tag{2}$$

where f_{Ni} is the axial force of the i^{th} limb, L_i is the length of the i^{th} limb, E_i is the elastic modulus of the i^{th} limb, and A_i is the cross-sectional area of the i^{th} limb. The total strain energy of the mechanism can be obtained as

$$U = \sum_{i=1}^{6} U_i = \sum_{i=1}^{6} \frac{f_{Ni}^2 L_i}{2E_i A_i}. \tag{3}$$

The elastic deformation of the limb end along the direction of the constraint wrench screw system is obtained from Castigliano's second theorem and the relation

$$\delta_i = \frac{\partial U_i}{\partial f_i} = \frac{L_i}{E_i A_i} f_i. \tag{4}$$

The screw flexibility matrix of the constraint system of the supporting limb is obtained as

$$C_i = \frac{L_i}{E_i A_i}. \tag{5}$$

And the screw stiffness matrix of the constraint system is further obtained as

$$K_i = C_i^{-1}. \tag{6}$$

According to the giveCcn position and attitude, the compliance matrix of the SPS limb is $C_i = L_i/E_iA_i$, as expressed by equation (5). The stiffness matrix is $\mathbf{K}_i = C_i^{-1}$, where $\$_i^r = (s_i b_i \times s_i)$ is the unit screw of the constraint wrench vector direction applied by the ith limb to the mobile platform. S_i is the unit vector along the path of the A_iB_i rod, $b_i = pB_i$, and $J_i = (\$_i^r)$. S_i and b_i are expressed in the definite coordinate system o–xyz. The overall stiffness matrix K_i can thus be obtained from equation (6).

2.4. Overall Stiffness Matrix. The mobile platform equilibrium equation is

$$\mathbf{W} = \left(\ldots \$_{i1}^r \ldots \$_{ij}^r \ldots\right) f = G_f^E f, \tag{7}$$

Table 1: Physical and structural parameters of the 6-SPS PM.

Parameters	Units	Data
R	mm	200
r	mm	150
d	mm	60
E	GPa	210
G	GPa	80

Table 2: Configuration and external loads of the 6-SPS PM.

Parameters (meters)	Units	Pose 1	Pose 2	Pose 3	Pose 4	Pose 5
X	mm	0	0	0	0	−70
Y	mm	0	0	0	0	60
Z	mm	430	430	430	430	430
α	rad	0	pi/9	0	pi/9	0
β	rad	0	pi/9	0	pi/9	0
γ	rad	0	0	pi/9	0	0
F_x	N	0	0	1	1	1
F_y	N	0	0	1	1	1
F_z	N	−1	−1	−1	−1	−1
M_x	Nm	0	0	1	1	1
M_y	Nm	0	0	1	1	1
M_z	Nm	0	0	1	1	1

where $\mathbf{W} = [\mathbf{F}\ \mathbf{M}]$ is an extra wrench acting on the mobile platform and $\$_{ij}^r$ is the unit screw of the j^{th} constraint force that the i^{th} limb exerts on the mobile platform. $G_f^E f = (\ldots \$_{i1}^r \ldots \$_{ij}^r \ldots)$ is a 6×6 matrix while $f = (\ldots f_{i1} \ldots f_{ij} \ldots)^T$ is a 6×1 matrix.

Under the action of the constraint wrench screw, elastic deformation at the end of each limb of the mechanism is generated along the axis of the constraint wrench screw. The deformation coordination between the infinitesimal displacements of the mobile platform under the action of external forces is expressed as

$$\left(\delta_{i1} \ldots \delta_{ij}\right)^T = \left(\$_{i1}^r \ldots \$_{ij}^r\right)^T \mathbf{D} = J_i^T \mathbf{D}, \tag{8}$$

where $J_i = (\$_{i1}^r \ldots \$_{ij}^r)^T$ and $\mathbf{D}$ is the tiny twist of the geometric center point of the mobile platform. According to the knowledge of material mechanics, we have

$$\left(f_{i1} \ldots f_{ij}\right)^T = K\left(\delta_{i1} \ldots \delta_{ij}\right)^T, \tag{9}$$

Then, by substituting equations (8) and (9) into equation (7), we have

$$W = \left(\ldots \$_{i1}^r \ldots \$_{ij}^r\right) f = \sum_{i=1}^{n} \left[\left(\$_{i1}^r \ldots \$_{ij}^r\right) W = \left(f_{i1} \ldots f_{ij}\right)^T\right], \\ = \sum_{i=1}^{n} J_i K_i J_i^T \mathbf{D} = K\mathbf{D}, \tag{10}$$

$$K = \sum_{i=1}^{n} J_i K_i J_i^T, \tag{11}$$

where n is the number of limbs of the Stewart PM. Equation (11) is the general analytical expression of the overall

Table 3: Deformation of the geometric center point of the mobile platform of the 6-SPS PM (comparison of the results of the FEA and theoretical models).

Pose	Method	δx (mm) ($\times 10^{-4}$)	δy (mm) ($\times 10^{-4}$)	δz (mm) $\times 10^{-5}$)	$\delta\theta_x$ (rad) ($\times 10^{-7}$)	$\Delta\theta_y$ (rad) ($\times 10^{-7}$)	$\Delta\theta_z$ (rad) ($\times 10^{-7}$)
1	Theoretical model	$-1.066e-17$	$-3.272e-17$	-0.173	$8.338e-18$	$-4.254e-17$	$1.665e-16$
	FEA results	$-0.199e-7$	$0.345e-7$	-0.175	$0.212e-6$	$0.122e-6$	$-0.551e-13$
	Relative error (%)	—	—	1.297	—	—	—
2	Theoretical model	-0.0012691	0.0091930	-0.15982	0.014668	-0.0014667	-0.048271
	FEA results	-0.0012843	0.0093202	-0.16190	0.014880	-0.0014839	-0.048905
	Relative error (%)	1.1835	1.3648	1.2847	1.4247	1.1591	1.2964
3	Theoretical model	0.63848	0.63894	-0.17272	0.23141	-0.22817	0.014194
	FEA results	0.64688	0.64735	-0.17499	0.23445	-0.23117	0.014386
	Relative error (%)	1.2985	1.2991	1.1429	1.2821	1.2987	1.3889
4	Theoretical model	0.752	0.585	-0.239	0.0732	-0.388	-1.37
	FEA results	0.762	0.593	-0.242	0.0742	-0.393	-1.39
	Relative error (%)	1.3123	1.3491	1.2397	1.3477	1.2723	1.4388
5	Theoretical model	0.577	0.730	-0.261	0.248	-0.249	0.0431
	FEA results	0.585	0.739	-0.264	0.251	-0.253	0.0436
	Relative error (%)	1.3675	1.2179	1.1364	1.1952	1.5810	1.1468

stiffness matrix and is more concise. The analytical model of the stiffness matrix is given from the perspective of strain energy and Castigliano's second theorem.

2.5. Amplitude of the Driving Force. From equation (10), we further obtain

$$\mathbf{D} = K^{-1}\mathbf{W}. \tag{12}$$

Then, by substituting equations (8) and (12) into equation (9), we obtain the inverse constrained solution equation as

$$\left(f_{i1} \cdots f_{ij}\right)^T = K_i J_i^T K^{-1}\mathbf{W}. \tag{13}$$

2.6. Comparison with the Virtual Joint Method. According to the calculation requirements of the VJM, the rod is regarded as a rigid rod, supported by a virtual spring at both ends of the rod. The limb of the SPS can be treated as a two-force rod, and the virtual spring is a one-way spring along the axial direction of the rod. The stiffness coefficient of the spring is

$$\mathbf{K}_i = \frac{\mathbf{EA}}{\mathbf{L}_i}. \tag{14}$$

The overall stiffness matrix $\mathbf{K}$ is

$$\mathbf{K} = \sum_{i=1}^{6} \mathbf{K}_i \mathbf{J}_i \mathbf{J}_i^T. \tag{15}$$

Formally, equation (15) is the same as equation (11). Due to the fact that the VJM method cannot calculate the strain energy stored in each rod, the method proposed in this paper can calculate the strain energy stored in each rod and overall parallel manipulators. A new approach to solving the problem of each component for the stiffness performance of the PM is proposed.

3. Comparison of the Proposed Model and FEA Model

The finite-element commercial software ANSYS is used to develop a unified FEA model and verify the correctness and feasibility of the method investigated in this paper. Analytical expression theory and the FEA simulation model are implemented.

Physical parameters of the 6-SPS PM are given in Table 1, where R is the radius of the circumferential circle of the fixed platform, r is the radius of the circumferential circle of the mobile platform, d is the diameter of the cross section of the limb rod, and E and G are, respectively, the elastic modulus and shear modulus of the material.

At the same time, the five poses and five groups of external forces and their couples acting on the mobile platform of the 6-SPS PM are given in Table 2.

Five groups of data to make a theoretical analysis calculation and FEA simulation calculation for the established analytical model are taken. The results obtained using the two methods are compared one by one. The theoretical calculation values, FEA simulation values, and relative errors of each group are listed in Table 3. It shows that the maximum relative error is 1.581% for the fifth group. All relative errors between the results of the analytical model and the workbench finite element model are below 2%, which validates the effectiveness of the proposed elastostatic stiffness model of the 6-SPS PM.

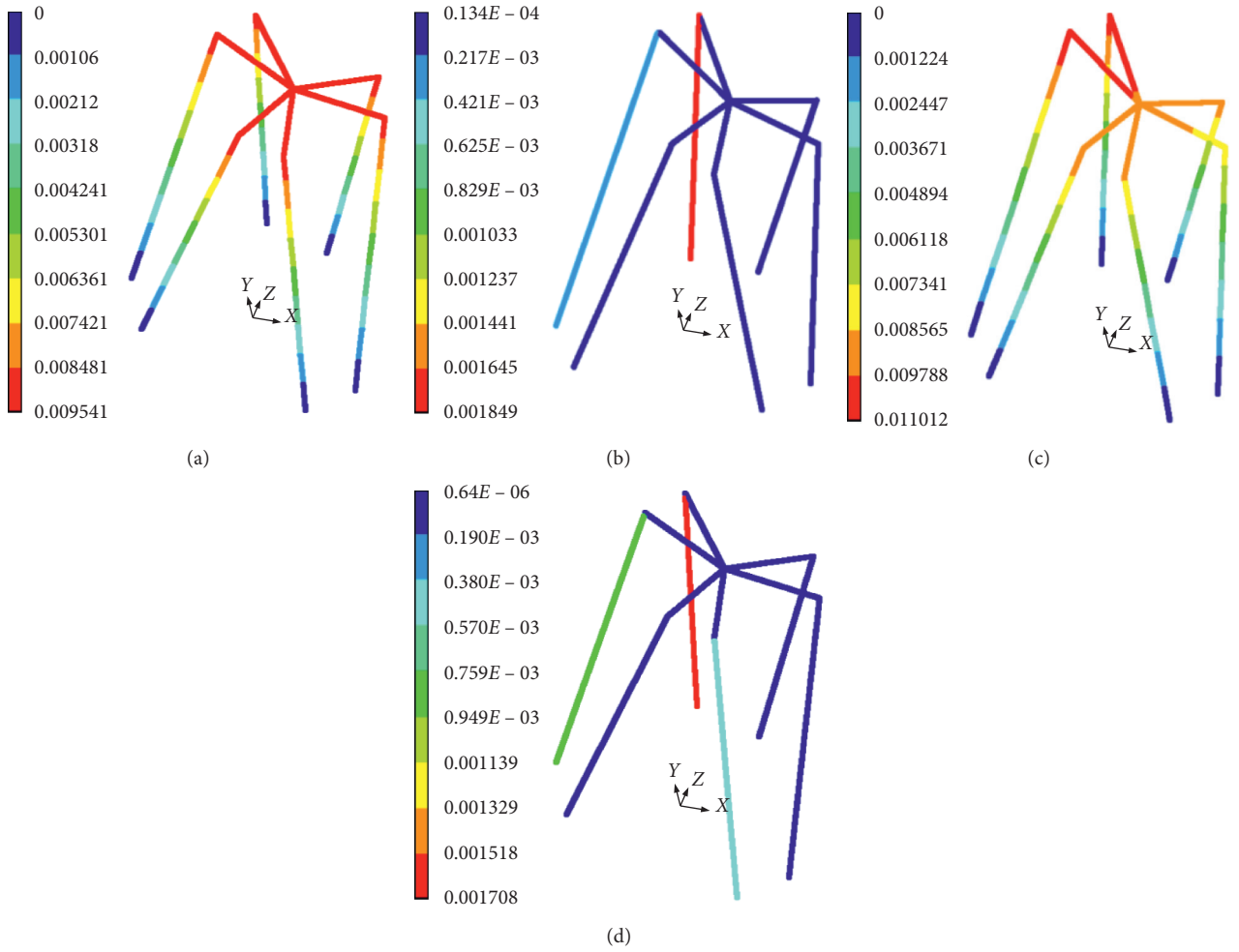

FIGURE 6: FEA simulation calculation of (a) the stiffness for pose 2 angle change, (b) the stiffness for pose 3 displacement change, (c) the stiffness for pose 3 angle change, and (d) the stiffness for pose 4 displacement change.

4. Stiffness Index of the 6-SPS PM

The VWI is used to evaluate the stiffness of PMs. In contrast with other indices, this index unifies the units of displacement and angle relating to virtual work. By correlating the value of the stiffness index with the direction of the external load, the ability of the mechanism to resist the external load in one direction is measured.

Supposing that a unit wrench W is imposed on the mobile platform, the virtual work done by the unit wrench can be expressed as

$$\mathbf{W}_V = \mathbf{W}^T \delta\xi. \tag{16}$$

The infinitesimal twist is $\delta\xi = K^{-1}\mathbf{W}$, and the VWI of the stiffness for the 6-SPS can thus be expressed as

$$VW = \frac{1}{\mathbf{W}^T K^{-1} \mathbf{W}}. \tag{17}$$

The VWI of the stiffness for the 6-SPS PM is a measure of the ability of the mechanism to resist deformation under a given external wrench. It allows the stiffness matrix to be transformed into a single index value. To calculate the value of the VWI, the virtual work completed by the force and moment must have the same units.

5. Results and Discussion of the Simulation

For the convenience of research, the unit of virtual work in the calculation process is uniformly adopted as 0.001 J. The distribution of the VWI of the 6-SPS PM in the plane $\mathbf{z} = 430$ mm, when $\mathbf{W} = [0\ 0\ -1\ 0\ 0\ 0]^{\mathrm{T}}$ and $\mathbf{W} = [0.4082;\ 0.4082;\ 0.4082;\ 0.4082;\ 0.4082]^{\mathrm{T}}$. The VWI of the stiffness for the Stewart PM changes with x and y, as shown in Figures 6(a) and 6(b), and index value changes with pose, as shown in Figures 6(c) and 6(d).

Under the vertical load, Figures 7(a) and 7(c) show the VWI of the stiffness for the 6-SPS PM that has a symmetrical distribution. The results are consistent with the fact that the mechanism is symmetrical. The stiffness index presents a different distribution under the action of external loads in

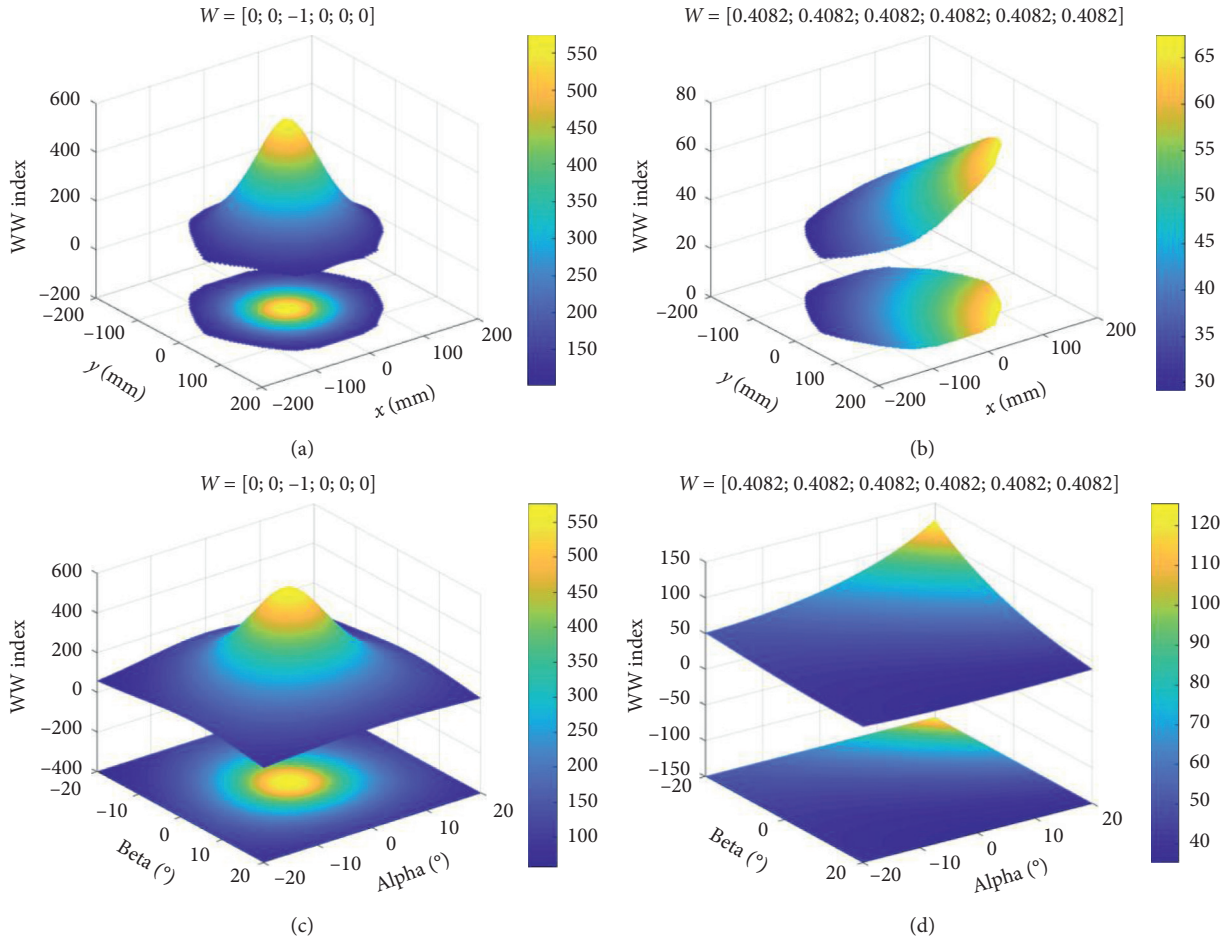

Figure 7: Distribution of changes in the VWI with the values of x and y for the 6-SPS PM in the plane $z = 430$ when (a) $\mathbf{W} = [0\ 0\ -1\ 0\ 0\ 0]^{\mathrm{T}}$, (b) $\mathbf{W} = [0.4082;\ 0.4082;\ 0.4082;\ 0.4082;\ 0.4082]^{\mathrm{T}}$, (c) $\mathbf{W} = [0\ 0\ -1\ 0\ 0\ 0]^{\mathrm{T}}$, and (d) $\mathbf{W} = [0.4082;\ 0.4082;\ 0.4082;\ 0.4082;\ 0.4082]^{\mathrm{T}}$.

different directions. Figure 7(a) shows the results for a vertical load. The stiffness of the 6-SPS PM is best for the central position, and the stiffness performance of the mechanism decreases rapidly with deviation from this position.

Similarly, we can see from Figure 7(c) that the stiffness performance of the 6-SPS PM is best when the position is not deflected, and the stiffness performance of the mechanism decreases rapidly with deviation from this position.

Figures 7(b) and 7(d) show that the optimal position for the 6-SPS PM stiffness under random loading is not at the central position of the mechanism. The results show that the stiffness performance of the 6-SPS PM is closely related to the direction of the external load and different under different external loads. It is shown that the elastic deformation of the 6-SPS PM is closely associated with the stiffness, configuration, and external loads.

6. Conclusion

In this work, a modeling method is investigated for elastostatic stiffness analysis for the UP/UPS PMs, taking the example of the 6-SPS PM, which is based on the screw theory, Castigliano's theorem, and strain energy method. The global stiffness matrix was derived. The virtual work index was adopted to evaluate the stiffness of the 6-SPS PM, and the VWI was used to measure the deformation of the 6-SPS PM in resisting external loads in specific directions. The main conclusions of the study are as follows:

(1) Although the theoretical method used in this paper is much simplified and has many limitations, the results show that the relative errors of the theoretical model and finite element model are less than 2%, which verifies the correctness of the analytical model. During the predesign stage, the stiffness analysis model used in this paper can be regarded as an alternative to the finite element model in evaluating the stiffness performance of the 6-SPS PM.

(2) The VWI was used to evaluate the stiffness performance of the 6-SPS PM. The results show that the stiffness of the mechanism is related to the direction of the action of the external wrench.

(3) In contrast, VJM cannot calculate the strain energy stored in each rod, and the described method can be applied to not only the 6-SPS PM but also other US/UPS PMs, such as two-DOF PMs, three-DOF PMs, and other six-DOF PMs.

The modeling method for the elastostatic stiffness of the US/UPS PMs was derived in this paper. The limitation of the model is that the flexibility of a joint is ignored. The study did not establish an experimental model for verification and did not consider the problem of dynamics. These issues need further study in the future.

Data Availability

The MATLAB and ANSYS files data used to support the findings of this study are available from the corresponding author upon request.

Conflicts of Interest

The authors declare that they have no conflicts of interest.

Acknowledgments

The authors thank the Robot Research Group of Zhejiang Sci-Tech University, Hangzhou, China, which supported them in theoretical guidance. This research was supported by the Basic Public Welfare Research Project of Zhejiang Province, China (Grant no. LGG19E050018), the Open Foundation of the Most Important Subjects of Zhejiang Sci-Tech University (Grant no. ZSTUME01A07), the Major Research Development of Incubation Projects of the Zhejiang Institute of Mechanical and Electrical Engineering (Grant no. A027118106), and the Public Welfare Research Project of Jiaxing City, Zhejiang Province, China (Grant no. 2020AY10013).

References

[1] H. Qiang, L. Wang, J. Ding, and L. Zhang, "Multiobjective optimization of 6-DOF parallel manipulator for desired total orientation workspace," *Mathematical Problems in Engineering*, vol. 2019, pp. 1–10, Article ID 5353825, 2019.

[2] Z. Huang and Q. C. Li, "Type synthesis of symmetrical lowermobility parallel mechanisms using the constraint-synthesis method," *The International Journal of Robotics Research*, vol. 22, no. 1, pp. 59–79, 2003.

[3] C. M. Gosselin and É. S. Pierre, "Development and experimentation of a fast 3-DOF camera-orienting device," *The International Journal of Robotics Research*, vol. 16, no. 5, pp. 619–630, 1997.

[4] T. St-Pierre, M. Li, Z. Li, D. G. Chetwynd, and D. J. Whitehouse, "Optimal kinematic design of 2-DOF parallel manipulators with well-shaped workspace bounded by a specified conditioning index," *IEEE Transactions on Robotics and Automation*, vol. 20, no. 3, pp. 538–543, 2004.

[5] X. Chai, J. N. Xiang, and Q. C. Li, "Singularity analysis of a 2-UPR-RPU parallel mechanism," *Journal of Mechanical Engineering*, vol. 51, no. 13, pp. 144–151, 2015.

[6] Z. Chen, L. Xu, W. Zhang, and Q. Li, "Closed-form dynamic modeling and performance analysis of an over-constrained 2PUR-PSR parallel manipulator with parasitic motions," *Nonlinear Dynamics*, vol. 96, no. 1, pp. 517–534, 2019.

[7] D. Zhang and B. Wei, "Interactions and optimizations analysis between stiffness and workspace of 3-UPU robotic mechanism," *Measurement Science Review*, vol. 17, no. 2, pp. 83–92, 2017.

[8] G. Wu and P. Zou, "Comparison of 3-DOF asymmetrical spherical parallel manipulators with respect to motion/force transmission and stiffness," *Mechanism and Machine Theory*, vol. 105, pp. 369–387, 2016.

[9] C. Menon, R. Vertechy, M. C. Markot, and V. Parenti-Castelli, "Geometrical optimization of parallel mechanisms based on natural frequency evaluation: application to a spherical mechanism for future space applications," *IEEE Transactions on Robotics*, vol. 25, no. 1, pp. 12–24, 2014.

[10] B. Ding, R. M. Stanley, B. S. Cazzolato, and J. J Costi, "Real-time FPGA control of a hexapod robot for 6-DOF biomechanical testing," in *Proceedings of the 37th Conference of the IEEE Industrial Electronics Society*, pp. 252–257, IEEE, Melbourne, Australia, November 2005.

[11] V. E. Gough and S. G. Whitehall, "Universal tire test machine," in *Proceedings 9th International Technical Congress FISITA*, vol. 117, pp. 117–135, London, UK, 1962.

[12] V. E. Ömürlü and İ. Yildiz, "Parallel self-tuning fuzzy PD + PD controller for a stewart-gough platform-based spatial joystick," *Arabian Journal for Science and Engineering*, vol. 37, no. 7, pp. 2089–2102, 2012.

[13] D. Stewart, "A platform with six degrees of freedom," *Aircraft Engineering and Aerospace Technology*, vol. 38, no. 4, pp. 30–35, 1966.

[14] F. B. Afzali and P. Lidström, "A joint-space parametric formulation for the vibrations of symmetric gough-stewart platforms," *Progress in Systems Engineering: Proceedings of the Twenty-Third International Conference on Systems Engineering*, pp. 323–329, Springer, Cham, Switzerland, 2015.

[15] Q. Liang, D. Zhang, Z. Chi, Q. Song, Y. Ge, and Y. Ge, "DOF micro-manipulator based on compliant parallel mechanism with integrated force sensor," *Robotics and Computer-Integrated Manufacturing*, vol. 27, no. 1, pp. 124–134, 2011.

[16] B. Song and T. S. Mruthyunjaya, "The Stewart platform manipulator: a review," *Mechanism and Machine Theory*, vol. 35, no. 1, pp. 15–40, 2000.

[17] D. C. Zhu, W. H. Zhan, F. P. Wu, and A. Simeone, "T topology optimization of spatially compliant mechanisms with an isomorphic matrix of a 3-UPC type parallel prototype manipulator," *Micromachines*, vol. 9, no. 4, p. 184, 2018.

[18] C. Innocenti and V. Parenti-Castelli, "Echelon form solution of direct kinematics for the general fully-parallel spherical wrist," *Mechanism and Machine Theory*, vol. 28, no. 4, pp. 553–561, 1993.

[19] Y Lu, Z. Dai, and N. Ye, "Stiffness analysis of parallel manipulators with linear limbs by considering inertial wrench of moving links and constrained wrench," *Robotics and Computer-Integrated Manufacturing*, vol. 46, pp. 58–67, 2017.

[20] E. Javad and A. A. Tootoonchi, "Accuracy and stiffness analysis of a 3-RRP spherical parallel manipulator," *Robotica*, vol. 29, no. 2, pp. 193–209, 2011.

[21] S. Fan and S. Fan, "Difference between the ideal and combined spherical joints and its effects on parallel manipulators," *Proceedings of the Institution of Mechanical Engineers, Part C: Journal of Mechanical Engineering Science*, vol. 234, no. 5, pp. 1112–1129, 2020.

[22] S. Fan, S. Fan, W Lan, and G. Song, "A new approach to enhance the stiffness of heavy-load parallel robots by means of the component selection," *Robotics and Computer-Integrated Manufacturing*, vol. 61, Article ID 101834, 2020.

[23] C. Chen, F. Peng, R. Yan et al., "Stiffness performance index based posture and feed orientation optimization in robotic milling process," *Robotics and Computer-Integrated Manufacturing*, vol. 55, pp. 29–40, 2019.

[24] G. Li and L. S. Haynes, "Six-degree-of-freedom active vibration isolation using a Stewart platform mechanism," *Journal of Field Robotics*, vol. 10, no. 5, pp. 725–744, 1993.

[25] Z. Niu, Y. Zhao, T. Zhao, Y. Cao, and M. Liu, "Measurement model and calibration experiment of over-constrained parallel six-dimensional force sensor based on stiffness characteristics analysis," *Measurement Science and Technology*, vol. 28, no. 10, Article ID 105104, 2017.

[26] T. D. Liu, B. Li, and N. Wang, "Analysis and optimization of a vibration isolation platform based on 6-DOF parallel mechanism," *Key Engineering Materials*, vol. 625, pp. 748–753, 2014.

[27] B. Ding, B. S. Cazzolato, S. Grainger, R. M. Stanley, and J. J. Costi, "Active preload control of a redundantly actuated stewart platform for backlash prevention," *Robotics and Computer Integrated Manufacturing*, vol. 32, pp. 11–24, 2015.

[28] H. Adam, M. Hesselroth, and P. Hennessey, "Analytical evaluation of the double Stewart platform tensile truss stiffness matrix," *Journal of Mechanisms and Robotics*, vol. 6, no. 1, Article ID 101103, 18 pages, 2014.

[29] X. Li, S. Dai, and R. Zeng, "UKF based filtering and curve fitting for estimating the joint stiffness of stewart platform," in *Proceedings of IEEE Chinese Guidance, Navigation and Control Conference*, pp. 12–14, IEEE, Nanjing, China, August, 2016.

[30] M. M. Svinin, S. Hosoe, and M. Uchiyama, "On the stiffness and stability of gough-stewart platforms," in *Proceedings of IEEE International Conference on Robotics and Automation*, pp. 21–26, IEEE, Seoul, South Korea, May, 2001.

[31] C. T. Huang, W. H. Hung, and I. Kao, "New conservative stiffness mapping for the stewart-gough platform," in *Proceedings of IEEE International Conference on Robotics and Automation*, pp. 11–15, IEEE, Washington, DC, USA, May, 2002.

[32] H. Liu, T. Huang, D. G. Chetwynd, and A. Kecskemethy, "Stiffness modeling of parallel mechanisms at limb and joint/link levels," *IEEE Transactions On Robotics*, vol. 33, no. 3, pp. 734–741, 2017.

[33] İ. Görgülü, G. Carbone, and M. İ. C. Dede, "Time efficient stiffness model computation for a parallel haptic mechanism via the virtual joint method," *Mechanism and Machine Theory*, vol. 143, Article ID 103614, 2020.

[34] Y. W. Li, J. S. Wang, and L. P. Wang, "Stiffness analysis of a Stewart platform-based parallel kinematic machine," in *Proceedings of IEEE International Conference on Robotics and Automation*, pp. 11–15, IEEE, Washington, DC, USA, May, 2002.

[35] S. J. Yan, S. K. Ong, and A. Y. C Nee, "Stiffness analysis of parallelogram-type parallel manipulators using a strain energy method," *Robotics and Computer-Integrated Manufacturing*, vol. 37, pp. 13–22, 2016.

[36] S.-F. Chen, "The spatial conservative congruence transformation for manipulator stiffness modeling with coordinate and noncoordinate bases," *Journal of Robotic Systems*, vol. 22, no. 1, pp. 31–44, 2005.

[37] H. Tari, H.-J. Su, and J. D. Hauenstein, "Classification and complete solution of the kinetostatics of a compliant stewart-gough platform," *Mechanism and Machine Theory*, vol. 49, pp. 177–186, 2012.

[38] E. Courteille, D. Deblaise, and P Maurine, "Design optimization of a delta-like parallel robot through global stiffness performance evaluation," in *Proceedings of IEEE/RSJ International Conference on Intelligent Robots and Systems*, pp. 11–15, IEEE, Louis, MO, USA, October, 2009.

[39] Q. Xu and Y. Li, "GA-based architecture optimization of a 3-PUU parallel manipulator for stiffness performance," in *Proceedings of the 6th World Congress on Intelligent Control and Automation*, vol. 2, pp. 9099–9103, IEEE, Dalian, China, June 2006.

[40] B. S. El-Khasawneh and P. M. Ferreira, "Computation of stiffness and stiffness bounds for parallel link manipulators," *International Journal of Machine Tools and Manufacture*, vol. 39, no. 2, pp. 321–342, 1999.

[41] C. Gosselin and J. Angeles, "A global performance index for the kinematic optimization of robotic manipulators," *Journal of Mechanical Design*, vol. 113, no. 3, pp. 220–226, 1991.

[42] C. Yang, Q. Li, Q. Chen, and L. Xu, "Elastostatic stiffness modeling of overconstrained parallel manipulators," *Mechanism and Machine Theory*, vol. 122, no. 122, pp. 58–74, 2018.

[43] R. Vertechy and V. Parenti-Castelli, "Static and stiffness analyses of a class of over-constrained parallel manipulators with legs of type US and UPS," in *IEEE International Conference on Robotics and Automation*, pp. 10–14, IEEE, Roma, Italy, April, 2007.

[44] H. Tian, C. Wang, X. Dang, and L. Sun, "6-DOF parallel bone-grinding robot for cervical disc replacement surgery," *Medical & Biological Engineering & Computing*, vol. 55, no. 12, pp. 2107–2121, 2017.